CONFERENCE SUBMISSION

Lattice Optimization for Designing Diabetic Ulcer Orthotics

Optimizing Lattice Geometries for Enhanced Orthotic Insole Performance in Diabetic Ulcer Management

Authors 1 Name: Chakraboon Bhanarai,

Name/s per 2nd Affiliation *(Author)*

Dept. Biomedical Engineering Research Center (BMERC)

Chulalongkorn University (CU)

Bangkok, Thailand

contact: chakraboon.b@gmail.com

***Abstract*—Diabetic foot ulcers represent a critical medical challenge, requiring effective orthotic solutions to alleviate pressure and promote healing. This study explores the design and optimization of six lattice structures fabricated via additive manufacturing, aimed at improving the mechanical properties of orthotic insoles, in support towards diabetic ulcer patients at Chulalongkorn Hospital. Using Fusion 360, three distinct lattice geometries were designed, categorized as Lattice "Hexagon," "Hourglass," and "Spring." Each design is differentiated by an independent variable "Lattice Poisson Ratio." Measurements were made on the controls of the experiment (lattice density gradients, force placed, and lattice dimensions). These 3 designs are designed using 2 different printing devices: Bambu Slicer Lab A1 0.4mm, and Original Prusa i3 Mk3 0.2mm QUALITY. Numerical analyses of compressive stress-strain can determine mechanical properties of the Poisson's ratio conducted. Results show significant variations in performance based on lattice geometry and fabrication methods, providing actionable insights for orthotic insole optimization. Further evaluation into the extension of this study can be conducted regarding stress-strain consistency, and vitally cracking and material durability.**

***Index Terms*— Diabetic Foot Ulcers, Orthotic Devices, Lattice Structures, Insoles, Fusion 360, Logger Pro, Poisson's Ratio, Instron Machine, Compressive Stress-Strain, Axial Strain, Transverse Strain, Numerical Analysis.**

I. Introduction

The increasing prevalence of diabetes has brought attention to its severe complications, among which diabetic foot ulcers stand out as a critical challenge. These ulcers not only compromise patient mobility but also carry a high risk of infection, potentially leading to amputation. As such, there is a pressing need for innovative solutions to mitigate these risks. Orthotic insoles have emerged as a key intervention, capable of redistributing plantar pressure and alleviating strain on ulcer-prone areas.

This study explores the integration of lattice structures in orthotic insole design to address the mechanical challenges posed by diabetic ulcers. Leveraging the precision and versatility of additive manufacturing, this research investigates how variations in lattice geometry and density can optimize pressure redistribution. By examining different lattice configurations and fabrication methods, the study aims to provide actionable insights for enhancing orthotic performance and improving patient outcomes.

II. Background Information

A. Diabetic Foot Ulcers

Diabetic foot ulcers are among the most severe complications associated with diabetes mellitus, affecting up to 25% of patients during their lifetime. These ulcers significantly impair quality of life and can lead to lower extremity amputations if not properly managed. The primary cause of these ulcers is elevated plantar pressure, often exacerbated by neuropathy and peripheral arterial disease. (Danko et al., 2023) Effective management strategies focus on offloading pressure from ulcer-prone areas, with orthotic insoles playing a crucial role. (Zoboli et al., 2024)

B. The Role of Orthotic Insoles

Orthotic insoles are widely used to distribute plantar pressure and prevent ulceration. Traditional insoles are made from materials such as ethylene-vinyl acetate (EVA), which provide cushioning but lack tunable mechanical properties. (Sterman et al., 2024) Advances in design and manufacturing techniques have enabled the creation of customized insoles that cater to the specific needs of diabetic patients. Lattice structures offer significant advantages due to their ability to provide both strength and flexibility, making them ideal for redistributing pressure while maintaining support.

C. Lattice Structures in Biomedical Applications

Lattice structures are a class of porous materials characterized by repeating unit cells. Their unique mechanical properties, including high strength-to-weight ratio and energy absorption capabilities, have made them a focus of research in biomedical engineering. In orthotic applications, lattice structures enable precise control over stiffness and flexibility, which are critical for ensuring comfort and effectiveness. (Sarinnapakorn et al., 2016)

D. Additive Manufacturing for Lattice Fabrication

Additive manufacturing (AM) technologies have revolutionized the production of complex geometries, including lattice structures. Fused deposition modeling (FDM), a widely used AM technique, allows for the fabrication of customized designs at relatively low cost. This study utilizes two FDM slicers—Bambu Slicer and Prusa Slicer—to fabricate lattice structures and compare their performance. (Kanna and Bala Vaidhyanathan, 2024)

The choice of slicer software significantly impacts the quality of the printed structure. Bambu Slicer is known for its high-resolution capabilities and precise layer bonding, while Prusa Slicer offers consistent performance but with potential variations in resolution and wall thickness. By analyzing the impact of these slicers on lattice performance, this research aims to identify optimal fabrication methods for orthotic insoles.

III. Optimization Parameters

There are 3 key variables considered through the process of cutting down on optimizing material print, design and property, when looking into this optimization process.

The following parameters determine the process that will follow within the methodology:

1. Lattice Dimension/Layering & Density (3-layered lattice structure)
2. Lattice Base-apex to Middle-apex Angle (μ)
3. Poisson's Ratio Customization
4. Lattice Slicing/Printing Versions & Presets

A. Lattice Dimension/Layering & Density

When discovering the optimal dimensions needed for a printed lattice cube, three consecutive tests were conducted. These lattices will be laid horizontally so two faces of the lattice cube will show the lattice structure pattern, whilst the rest of the faces will remain blank or the aftermath of scaffolded layers from the lattice designs. What faces will be made will depend on the lattice location within our theoretical orthotic, and the properties/strength of printing material or accuracy.

Using Fusion 360 and the 'Volumetric Lattice' preset, I designed a test module design, printing these test modules via Prusa Slicer & the Prusa Original Prusa i3 Mk3 0.2mm QUALITY, with a 90% printing speed. Initially, a 3 by 3-unit lattice formation under a 20.000mm by 20.000mm dimensions structure was printed, with no difference in printing of Density 0.250 defined from the volumetric lattice configurations

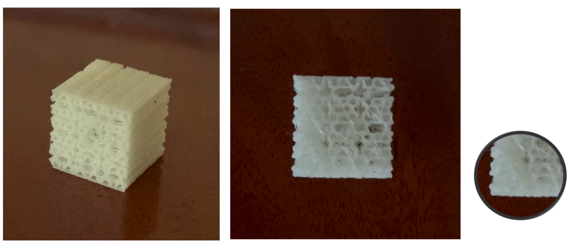

Figure 1a: 3 by 3 Unit Lattice 20m x 20m Lattice

The negative comments surrounding this lattice came due to the performativity of the lattice structures being too close together, and additionally the set 0.250 density uniformly distributed deemed impractical to distribute downward force.

I moved to a 3 by 3-unit lattice structure aligned with a 30.000mm by 30.000mm dimensional lattice structure, with uniformity in lattice density assigned, but assigned at 0.210.

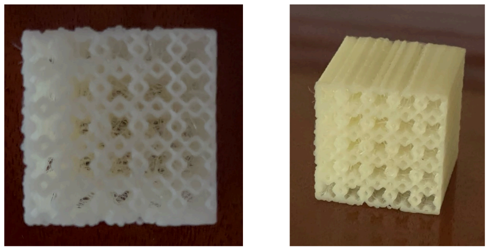

Figure 1b: 3 by 3 Unit Lattice 30m x 30m Lattice

This optimization pushed further towards a more performing lattice, as the spaced out 3 by 3-unit lattice allowed the lattice patterns to be adequately spaced for printing. What deemed a consistent struggle was the top layer lattice row (3 by 1 length-width unit lattice row) would perform adequate strain via uniform stress; however, the lower lattice would not perform similar response, even with a lower lattice density.

Hence, the final optimization consisted of separating each lattice row (3 by 1 length-width) into 3 separate lattice structures via Fusion 360, assigned with uniform density per-row, but distinct densities between each other, and to be merged within the slicing process. This optimization will demonstrate a difference of strain response within the entirety of the lattice due to this graduating layering, yet pertaining to optimal spacing of the lattice pattern, yet sustaining a deformation response over time.

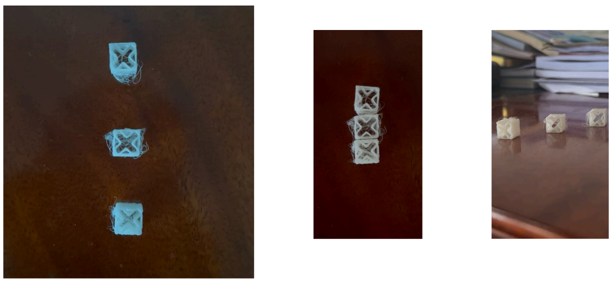

Figure 1c: 1 by 1 Unit Lattice 10m x 10m Lattice

Lastly, ***Figure 1c*** demonstrates the test unit lattice separated into three layers, sustaining the top, middle and bottom layers as 0.180, 0.230, & 0.280 Volumetric Lattice Densities (following a gradient subsequence of 0.050 additive per layer). Through this test, each individual lattice was able to demonstrate strain with the superimposition of lattice layers, however this signaled a change into the interval of subsequent layering. I shifted this preset to an additive interval of 0.0250.

B. Lattice Base-apex to Middle-apex Angle (Lattice BtM)

When looking at research focusing on the biomechanics of lattice geometries, the relationship between the apex angles and their capacity to endure compressive forces becomes a significant factor. Alterations in lattice apex angles affect strain distribution. These findings informed the design of three distinct lattice structures: “Hexagonal,” “Spring,” and “Hourglass.” By tuning the lattice base-apex to middle-apex angles (BtM), this study seeks to optimize deformation patterns under stress. These angles correlate directly to the Poisson’s ratio and thus influence the lattice's capacity to manage lateral and axial strains. Detailed specifications of the angle and geometry will be defined in the Fabrication Process.

I had designed three different lattice structures in differing lattice angles and based off these lattices to optimize a strain response from these lattices. I had designed the ‘Hexagonal,’ ‘Spring,’ and ‘Hourglass’ Lattices. Specifications in dimension and altercation will be defined in the Methodology.

When looking into this discovery, the Poisson’s Ratio was taken into consideration, into being able to optimize these lattice angles and pattern in defining different Poisson’s Ratios, to determine an exact performance deformation of each shape. This angle will be classified using the symbol μ.

1) Poisson’s Ratio

The Poisson ratio, in the orthotic pursuit in this case, is the fundamental material property defining the functionality styles through overhead deformation. This ratio is defined from the negative ratio between the change in lateral strain (transverse contraction) and change in longitudinal strain (axial extension) after an application of downward force on the lattice. (Nitta and Yam, 2012)

This is calculated by the following equation:

$$\nu = -\frac{d\varepsilon_{trans}}{d\varepsilon_{axial}}$$

where:
ν = Resultant Poisson’s Ratio
$d\varepsilon_{trans}$ = Transverse Strain
$d\varepsilon_{axial}$ = Axial Strain

In specific, the way in which these Poisson’s Ratio determine how a lattice deforms, can be defined under different Poisson’s Ratios:

1. Positive Poisson Ratio ($\nu > 0$): Compression leads to lateral expansion. In the context of foot soles, areas with a positive Poisson ratio can help relieve pressure, offering comfort in regions that experience regular stress.
2. Negative Poisson Ratio ($\nu < 0$): Compression results in lateral contraction, which can be strategically used in areas requiring greater support, such as around ulcer regions to prevent excessive movement and strain.
3. Zero Poisson Ratio ($\nu \approx 0$): No lateral change occurs during axial compression, maintaining the shape while providing consistent support.

(BYJU'S, n.d.)

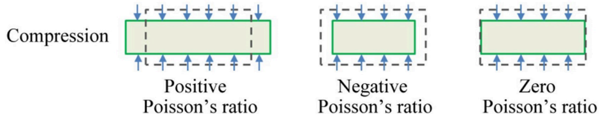

Figure 2: Theoretical Poisson’s Ratio Identification illustrating the behavior of materials under compression.

(Liu et al., 2020)

Pre-post displacement analysis is essential for ensuring that the insole can accommodate natural foot movements while providing necessary support. This analysis involves measuring the Poisson ratio before and after deformation to optimize the lattice structure for the specific biomechanical needs via the patients. (Lempriere, 2024)

These Poisson’s Ratios will be calculated with the collated changes in compression.

C. Filament Choice & Lattice Slicing/Printing Presets

One source of control for the exploration is the lattice material pertaining as TPU Filament. Specifically, the TPU Filament Model: 3D BAREfilament Flexible TPU Filament 1.75mm.

1) TPU Filament

Thermoplastic polyurethane (TPU) filament is a versatile, flexible material known for its durability, elasticity, and abrasion resistance. (Qi and Boyce, 2005) Its ability to withstand stretching and compressive forces makes it ideal for applications requiring resilience, such as lattices designed for mechanical testing. TPU combines the strength of rigid plastics with the flexibility of rubber, making it well-suited for experiments involving Poisson ratio analysis, as it allows for measurable deformation under axial and lateral stresses. (Perry et al., 2022) Printing with TPU requires careful calibration, as its flexible nature can lead to challenges like stringing or inconsistent extrusion if settings are not optimized. A slower print speed and precise filament retraction settings are typically recommended for high-quality results. TPU's unique properties make it particularly useful in fields such as biomedical devices, automotive components, and research focused on auxetic or deformable structures. (Aryabhat Darnal et al., 2023)

2) Flexible TPU Filament

Flexible TPU (Thermoplastic Polyurethane) filament is a durable, flexible, and weather-resistant material commonly used in 3D printing. It offers excellent elasticity and resilience, making it ideal for printing functional parts such as remote-control wheels and other components requiring flexibility. Compared to PLA, TPU is more heat-resistant and can endure prolonged exposure to high temperatures without deformation, making it suitable for applications like automotive interiors. It is easy to print with minimal shrinkage, does not require an enclosed printing environment, and produces no unpleasant odors during extrusion. With a printing diameter of 1.75mm ± 0.05mm, it is best printed at temperatures between 190–220°C and a bed temperature of 0–50°C. Print speeds of 20–50mm/s are recommended, depending on the printer's capabilities, for optimal results. TPU is available in both opaque and transparent options, offering versatility for different design needs. (Barefoot Filament, 2024)

These lattices will be printed into two sets, to introduce the parameter of specifying filament printing method. The two sets of the Printing Presets I have chosen are the Bambu Slicer Lab A1 0.4mm, and Original Prusa i3 Mk3 0.2mm QUALITY:

3) Bambu Slicer Lab A1 0.4mm

The Bambu Lab series, utilizing the Lab A1 0.4mm preset, is tailored for high-speed and efficient 3D printing, making it a strong candidate for rapid prototyping when looking to cut costs of TPU Filament usage. The 0.4mm nozzle balances speed and structural accuracy, enabling quick production of large lattice arrays where overall integrity matters more than fine details. Its CoreXY architecture minimizes vibrations during fast movements, and features like automatic calibration and multi-material compatibility enhance consistency and versatility. (3D DISTRIBUTED, n.d.) Optimized for faster build times, this preset is ideal for projects where testing of multiple iterations is required in a short time. However, the coarser layer height associated with this preset may slightly compromise finer geometries, which could influence detailed experimental outcomes, such as Poisson ratio measurements. (James Biggar, 2024) The Bambu Lab printer's cutting-edge technology reflects a modern, efficiency-driven approach, making it particularly suited for time-sensitive lattice experiments.

4) Original Prusa i3 Mk3 0.2mm QUALITY

The Original Prusa i3 Mk3, paired with the 0.2mm QUALITY preset, is renowned for its precision and reliability, excelling in applications where intricate detail and surface resolution are critical. This preset emphasizes higher resolution through finer layer heights and slower print speeds, making it ideal for capturing subtle features of lattice structures. Prusa's advanced features, including mesh bed leveling and filament monitoring, ensure consistent, error-free printing, even for detailed parts. (Prusa Research and Prusa, 2025) While print times are significantly longer compared to the Bambu Slicer Lab A1, the resulting parts are of research-grade quality, making this setup better suited for applications that demand detailed validation of lattice geometries and their behaviors under load. (ruiraptor, 2020) The Prusa i3 Mk3 represents a precision-focused, traditional approach to FDM printing, complementing the Bambu Lab by offering superior quality for deeper structural analysis.

IV. METHODOLOGY

A. Lattice Design Process

Three distinct lattice structures were designed using Fusion 360, and the depiction of Lattice 'BtM' angles identified that differ the compressive nature of the geometry.

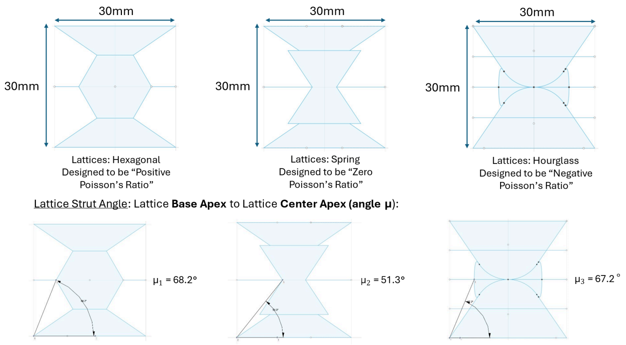

Figure 3: Fusion 360 Identification of Lattice Designs "Hexagonal," "Spring," & "Hourglass" respectively; Variance in Lattice Strut Angle to assume Poisson's Ratio

The geometries were fabricated in two batches: set {2, 3, 4} using Bambu Slicer Lab A1 0.4mm, and set {10, 8, 9} using Prusa Slicer, labeled sets respectively appealing to the order shown in ***Figure 3*** ('Hexagonal,' then 'Spring,' and then 'Hourglass.')

1) Lattice Layer Mesh Details

Using Fusion 360, I defined the respective volumetric lattices through the 'Volumetric Lattice' under the Fusion 360: Product Design Extension. Using the 'Solidify' option, adjustments in the density slider will differ the respective density layer increments for each layer {0.180, 0.205, 0.230}.

After defining the density, the thickness of the lattice default will have been varied, and hence rescaling with the 'Autoscaler' tool will fit the 3 by 1 length-width for each layer.

With the 'Offset Function', I will set upper and lower faces on top and bottom of the lattice itself, offsetting with a Density of 1.00, Blend Distance as minimal as possible (set 0.00001mm), in order to provide a printable layer for the lattice structures to work around the construction of each layer, and simulating upper and lower lattices of the insole.

These Lattices were then distributed via the 'Mesh Tessellation' selection of Fusion 360 for these layers. Each meshed body will be imported as .STL files to input into each respective slicer. The details of each mesh defined are in ***Figure 4a*** below.

Layer Name	**Hexagonal Lattice**		
Layer No.	**Layer 1**	**Layer 2**	**Layer 3**
Assigned Density	0.180	0.205	0.230
Offset Thickness	0.030	0.030	0.030
Mesh Mass (g)	0.017	0.021	0.024
Mesh Volume (mm ^{3})	2.140	2.640	3.210
Meshed Density (g mm ^{3})	0.00794	0.00795	0.00748
Mesh Area (mm^2)	95.494	93.549	90.149
Layer Name	**Spring Lattice**		
Assigned Density	0.180	0.205	0.230
Offset Thickness	0.030	0.030	0.030
Mesh Mass (g)	0.0140	0.0170	0.020
Mesh Volume (mm ^{3})	1.743	2.136	2.532
Meshed Density (g mm ^{3})	0.00803	0.00796	0.00790
Mesh Area (mm^2)	131.757	129.243	124.725
Layer Name	**Hourglass Lattice**		
Assigned Density	0.180	0.205	0.230
Offset Thickness	0.030	0.030	0.030
Mesh Mass (g)	0.019	0.023	0.027
Mesh Volume (mm ^{3})	2.422	2.967	3.494
Meshed Density (g mm ^{3})	0.00702	0.00775	0.773
Mesh Area (mm^2)	105.740	103.129	99.600

Figure 4a: Fusion 360 Volumetric Lattice & Mesh Tessellation Properties (3 D.P.)

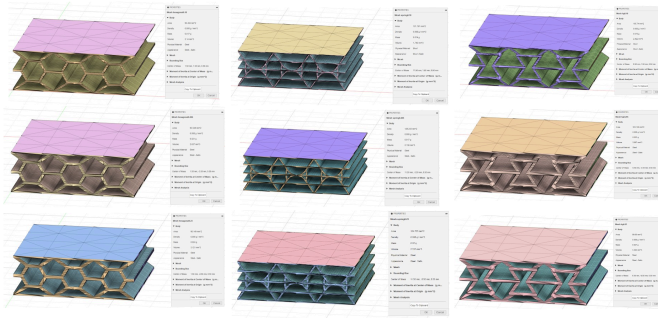

Figure 4b: Lattice Layer Mesh Details

B. Lattice Slice Process

Original Prusa i3 Mk4 0.4 Print Nozzle		
Specifications	Filament Used	Presetting
0.2mm QUALITY Print Nozzle Setting	Prusament PVB	No Supports 100% Infill
Bambu Slicer Lab A1 0.4mm Print Nozzle		
Specifications	Filament Used	Presetting
0.20mm Standard @ BBL A1	Bambu PLA Basic	No Supports Internal Solid Infill Pattern Rectilinear 100% Sparse Infill Density

Figure 4c: Lattice Slicer Properties, Filament & Presetting

These lattices are accumulated as ***Figure 4d*** from Fusion 360.

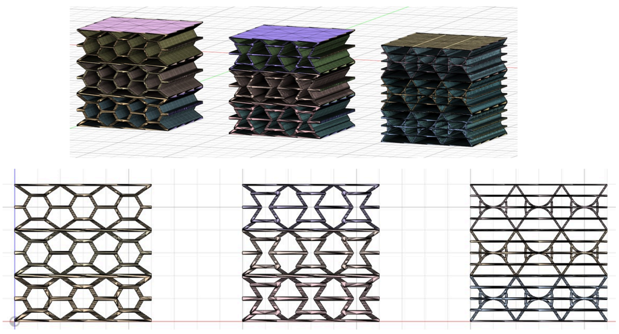

Figure 4d: Full Fusion 360 Lattice Details

C. Full Lattice Printed Figures & Lattice Designs Identification

Figure 5a shows the final models printed out.

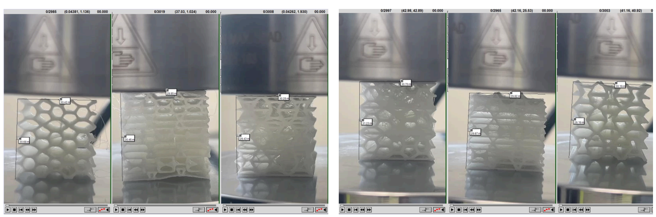

Figure 5a: Printed Figures of Lattice 2,3,4 (Bambu Slicer Lab A1 0.2mm) & Lattice 8,9,10 (Original Prusa i3 Mk3 0.2mm QUALITY) & Logger Pro Identification of Dimensions

(FIGURE 5a INCOMPLETE)

Post-print, these lattices were 'eye-test' identified in macroscopic measurements, then widened deeply through Logger Pro Graphical Analysis, serving as the preliminary for the Practical Conduction.

Lattice Design	X axis (in mm)	Y Axis (in mm)
Bambu Slicer Lab A1 0.4mm Print Nozzle		
Sample 2: Hexagonal	30.42	30.68
Sample 3: Spring	29.85	30.46
Sample 4: Hourglass	30.25	29.43
Original Prusa i3 Mk4 0.4 Print Nozzle		
Sample 10: Hexagonal	30.70	31.23
Sample 8: Spring	29.82	29.67
Sample 9: Hourglass	30.19	29.19

Figure 5b: Table of Details of Final Lattices from Logger Pro Identification

Figure 5b presents the comparative strain responses for the three-layered lattice structure when subjected to compressive forces. The graph highlights distinct strain behaviors for each layer—top, middle, and bottom—with varying lattice densities. The top layer, optimized at 0.180 volumetric density, demonstrates uniform strain absorption, while the middle and bottom layers, with densities of 0.230 and 0.280 respectively, show gradual increases in rigidity. This stratification ensures pressure redistribution across the lattice, preventing localized stress concentrations and enhancing insole durability. The analysis validates the gradient density approach, illustrating improved strain uniformity compared to non-gradient configurations.

D. Instron Universal Testing Machine Setup

Below is the identification of machinery setup & specimen visualization in setup:

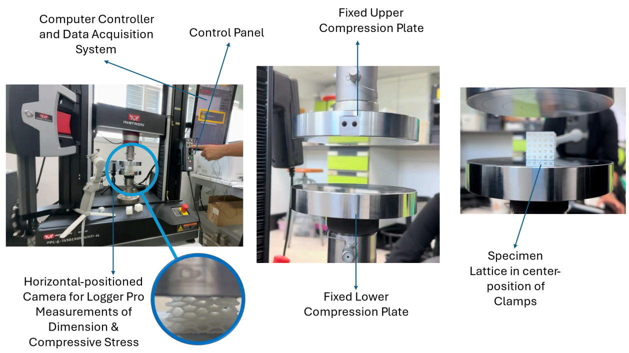

Figure 6: Instron 68TM-50 Universal Testing Machine Setup & Specimen Display

This Instron Universal Testing Machine 68TM-50 has the Compression Plate Preset, with 50kN Load Cell, and practical run of approximately 90 seconds.

E. Graphical Analysis

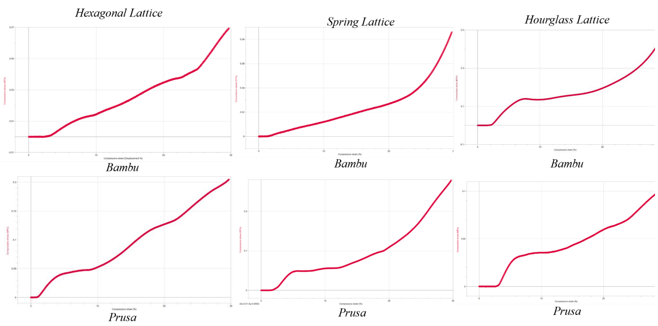

Figure 7: Comparative Printer Settings of Stress -Strain Analysis (Bambu TOP & Prusa BOTTOM)

F. Comparative of Parameter 3

Figure *7* illustrates the comparative stress-strain behavior of lattices fabricated using Bambu Slicer and Prusa Slicer under identical conditions. The data reveals that the Prusa-printed lattices consistently exhibit smoother stress-strain curves, indicative of more precise layer bonding and structural uniformity. This enhanced performance is especially apparent in the elastic deformation range, where Prusa lattices demonstrate lower hysteresis, suggesting superior energy efficiency during compression cycles.

In contrast, the Bambu-printed lattices, while adequate for rapid prototyping, show higher variability in their stress-strain responses. The observed inconsistencies, particularly in the plastic deformation range, highlight the trade-offs between faster printing speeds and reduced resolution. This variability can affect the reliability of the lattice under sustained loading conditions, making it less suitable for applications requiring precise mechanical behavior.

Overall, the findings emphasize the critical role of slicing presets in determining lattice performance. The Prusa Slicer's finer resolution ensures better mechanical consistency, making it the preferred choice for detailed orthotic applications. These insights provide a foundation for optimizing additive manufacturing parameters to achieve targeted stress-strain characteristics in lattice-based designs.

G. Prusa Models {10, 8, 9} Analysis

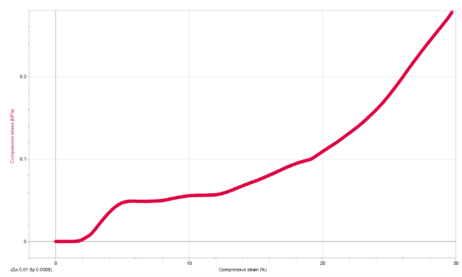

Figure 8a: Laboratory & Excel Analysis for Prusa Slice Lattice 8, graphed Compressive Stress [MPa] over Compressive Strain [%]

1) Model 10: Hexagonal Lattice (Figure 8a)

The stress-strain graph for Model 10 reveals a gradual linear deformation phase, indicative of its high strength-to-weight ratio. This behavior corresponds to a near-zero Poisson's ratio, meaning that the structure maintains its shape in the perpendicular direction under uniaxial stress. The elastic slope in the graph indicates significant rigidity, with limited lateral deformation. This geometry is ideal for distributing stress evenly, making it suitable for areas that require structural stability and minimal deformation.

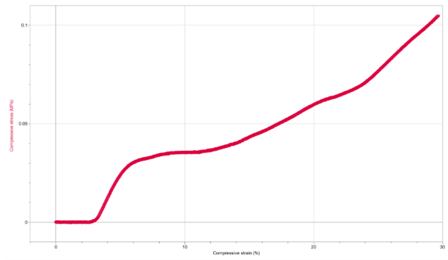

Figure 8b: Laboratory & Excel Analysis for Prusa Slice Lattice 9, graphed Compressive Stress [MPa] over Compressive Strain [%]

2) Model 8: Spring Lattice (Figure 8b)

The stress-strain graph for Model 8 demonstrates a nonlinear behavior, characterized by a steep elastic slope followed by a limited plateau region. This performance reflects a near-zero Poisson's ratio, where the lattice neither expands nor contracts laterally under axial compression. While the steep elastic slope highlights rigidity, the shorter plateau indicates constrained energy absorption. This lattice is best suited for applications where maintaining shape under load is crucial but where energy dissipation is not a primary requirement.

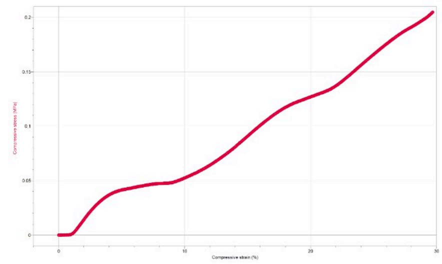

Figure 8c: Laboratory & Excel Analysis for Prusa Slice Lattice 10 graphed Compressive Stress [MPa] over Compressive Strain [%]

3) Model 9: Hourglass Lattice (Figure 8c)

The stress-strain graph for Model 9 exhibits a prolonged plateau region, characteristic of its auxetic behavior with a negative Poisson's ratio. As the lattice is compressed, it expands laterally, redistributing stress more effectively than conventional materials. The delayed densification and extended strain tolerance highlight its ability to absorb energy, making it ideal for cushioning and impact resistance. This unique combination of rigidity and flexibility is particularly advantageous for providing support in ulcer-prone regions while maintaining comfort.

H. Graphical Analysis of Axial-Lateral Compressive Strain Ratio

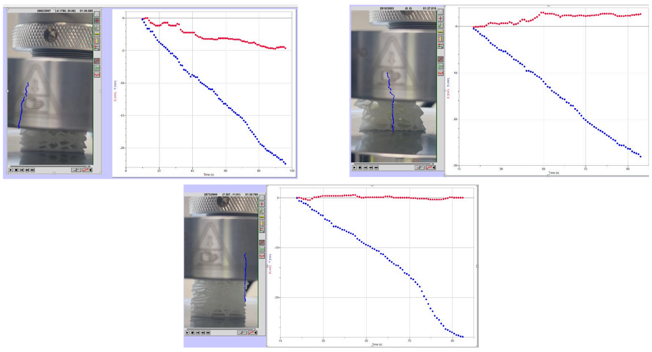

Figure 9: Logger Pro Identification of Axial Stress and Strain on 'Hexagonal,' 'Hourglass,' & 'Spring' Lattices

I. Numerical Analysis & Poisson's Ratio Calculations

For lattices with positive and zero Poisson's ratios, axial strain was calculated as:

$$v = -\frac{d\varepsilon_{trans}}{d\varepsilon_{axial}} = -\frac{(\frac{\Delta X}{X})}{(\frac{\Delta Y}{Y})}$$

$$\frac{\Delta X}{X} = \frac{X_0-(X_0+X)}{(X_0+X)})$$

where:

X_0 = Original Axial Measurement (values referenced in ***Figure 5b***)

X = Result Axial Contraction (measured from ***Figure 9***)

This equative process will also apply similarly to the $\frac{\Delta Y}{Y}$ property

However, for Negative Poisson's ratios:

$$v = -\frac{d\varepsilon_{trans}}{d\varepsilon_{axial}}$$

$$\frac{\Delta X}{X} = \frac{X_0-(X_0-X)}{(X_0-X)})$$

This negative sign refers to this difference: a negative Poisson's Ratio would need to define a contraction from the original axial measurement (hence contracting X_0 with X rather than being additive, which results as the Result Axial Contraction (X). (Dey, n.d.)

These Numerical Values are different from the Logger Pro Depictions, as these values of incremental X and Y changes, have been changed to be their absolute values, to show change rather than directional change due to how Logger Pro has measured lattice change.

X	Y	X	Y	X	Y	X	Y	X	Y	X	Y	X	Y	X	Y
0.178041543	0.2043543197	1.15727003	3.676164409	1.15727003	5.990704468	2.225519288	8.750348385	3.204747774	10.8868469	3.115727003	13.20138696	3.560830861	15.42690625	4.09495549	19.07675788
0.08902077151	0.6494581773	1.068249258	3.943226723	0.8902077151	6.257766783	2.225519288	8.928389928	3.204747774	10.97586767	3.115727003	13.46844928	3.560830861	15.78298933	4.272997033	19.43284097
0	1.094562035	0.8011869436	4.121268266	0.9792284866	6.791891412	2.581602374	9.106431471	3.204747774	10.97586767	3.204747774	13.82453236	3.649851632	16.05005165	4.362017804	19.61088251
0	1.628686664	0.7121661721	4.388330581	1.78041543	7.236995269	2.759643917	9.106431471	3.293768546	11.33195076	3.204747774	13.91355313	3.649851632	16.40613474	4.362017804	19.78892405
0.3560830861	1.628686664	0.7121661721	4.566372124	2.047477745	7.326016041	2.93768546	9.551535329	3.293768546	11.68803384	3.204747774	14.18061545	3.827893175	16.94025936	4.451038576	20.14500714
0.7121661721	2.073790521	0.7121661721	4.833434438	2.225519288	7.949161441	2.93768546	9.907618415	3.293768546	11.86607539	3.293768546	14.44767776	3.827893175	17.29634245	4.540059347	20.41206945
0.8011869436	2.073790521	1.068249258	5.100496753	2.225519288	8.038182213	3.115727003	10.08565996	3.115727003	12.40020002	3.293768546	14.6257193	3.827893175	17.56340476	4.629080119	20.50109022
0.9792284866	2.607915151	1.15727003	5.456579839	2.225519288	8.305244527	3.204747774	10.2637015	3.115727003	12.57824156	3.293768546	14.89278162	3.738872404	17.91948785	4.629080119	20.67913177
1.15727003	2.963998237	1.15727003	5.456579839	2.225519288	8.572306842	3.204747774	10.44174304	3.115727003	12.84530387	3.293768546	14.98180239	3.916913947	18.27557094	4.629080119	20.85717331
1.15727003	3.409102094	1.15727003	5.812662925	2.225519288	9.0174107	3.204747774	10.61978459	3.115727003	13.20138696	3.382789318	15.24886471	4.09495549	18.63165402	4.71810089	21.12423563

maxX	4.71810089
maxY	22.4595472
xorigin	yorigin
30.7	31.23
Axial Strain	-0.133212
Lateral Strain	30.23
Poisson's Ratio (v)	0.00441

Figure 10a: Excel Analysis of Displacement Change of Data Prusa Lattice 10 'Hexagonal' & Calculations of Axial Strain, Lateral Strain & Poisson's Ratio

1) Figure 10a: Hexagonal Lattice

The negative Poisson's ratio observed in ***Figure 10a*** highlights the auxetic nature of the hexagonal lattice. The axial and lateral strain calculations confirm its ability to expand laterally under axial compression, resulting in improved energy absorption and stress redistribution. This makes it suitable for high-impact applications where stability and adaptability are required.

X	Y	X	Y	X	Y	X	Y	X	Y	X	Y	X	Y	X	Y
0	0.0913916608	0.1827833216	3.107316467	0.3655666432	6.123241273	0	8.864991097	0.0913916608	11.33256594	0	15.07962403	0.1827833216	20.38034036	0.0913916608	26.50358163
0	0.6397416256	0.2741749824	3.47288311	0.3655666432	6.397416256	0	9.13916608	0.2741749824	11.78952424	0	15.26240735	0.2741749824	21.29425697	0.0913916608	26.77775661
0.0913916608	0.7311332864	0.3655666432	3.564274771	0.456958304	6.488807917	0.0913916608	9.413341062	0.2741749824	12.15509089	0	15.53658234	0.3655666432	22.20817357	0.0913916608	26.96053993
0.2741749824	1.09669993	0.3655666432	4.295408057	0.456958304	6.762982899	0.0913916608	9.596124384	0.2741749824	12.61204919	0.0913916608	16.17632396	0.3655666432	22.75652354	0	27.23471492
0.2741749824	1.18809159	0.3655666432	4.478191379	0.456958304	6.94576622	0.0913916608	9.778907705	0.1827833216	12.88622417	0.0913916608	16.35910728	0.3655666432	23.67044015	0	27.5088899
0.456958304	1.462266573	0.3655666432	4.660974701	0.456958304	7.128549542	0.0913916608	10.14447435	0	13.25179082	0.0913916608	16.90745725	0.3655666432	24.12739845	0	27.60028156
0.456958304	1.827833216	0.3655666432	5.117933005	0.5483499648	7.311332864	0.0913916608	10.32725767	0	13.5259658	0.1827833216	17.36441555	0.3655666432	24.49296509	0	27.78306488
0.1827833216	2.376183181	0.3655666432	5.75767463	0.5483499648	7.676899507	0.0913916608	10.60143265	0	13.61735746	0.1827833216	17.82137386	0.3655666432	25.22409838	0	27.87445654
0.0913916608	2.558966502	0.3655666432	5.75767463	0.2741749824	8.225249472	0.0913916608	10.69282431	0	14.07431576	0.1827833216	18.73529046	0.2741749824	25.68105668		
0.0913916608	2.741749824	0.3655666432	5.940457952	0.1827833216	8.499424454	0.0913916608	11.24117428	0	14.43988241	0.1827833216	19.74059873	0.1827833216	26.32079831		

maxX	0.5483499648
maxY	27.87445654
xorigin	yorigin
29.82	29.67
Axial Strain	-0.018057
Lateral Strain	28.67
Poisson's Ratio (v)	0.000630

Figure 10b: Excel Analysis of Displacement Change of Data Prusa Lattice 8 'Spring' & Calculations of Axial Strain, Lateral Strain & Poisson's Ratio

2) Figure 10b: Spring Lattice

Figure 10b reveals a near-zero Poisson's ratio for the spring lattice, indicating minimal lateral deformation during axial compression. The calculated axial and lateral strains align with the lattice's limited energy absorption capabilities, emphasizing its role in maintaining structural integrity without significant deformation.

X	Y	X	Y	X	Y	X	Y	X	Y	X	Y	X	Y	X	Y
0	0.0913916608	0.1827833216	3.107316467	0.3655666432	6.123241273	0	8.864991097	0.0913916608	11.33256594	0	15.07962403	0.1827833216	20.38034036	0.0913916608	26.50358163
0	0.6397416256	0.2741749824	3.47288311	0.3655666432	6.397416256	0	9.13916608	0.2741749824	11.78952424	0	15.26240735	0.2741749824	21.29425697	0.0913916608	26.77775661
0.0913916608	0.7311332864	0.3655666432	3.564274771	0.456958304	6.488807917	0.0913916608	9.413341062	0.2741749824	12.15509089	0	15.53658234	0.3655666432	22.20817357	0.0913916608	26.96053993
0.2741749824	1.09669993	0.3655666432	4.295408057	0.456958304	6.762982899	0.0913916608	9.596124384	0.2741749824	12.61204919	0.0913916608	16.17632396	0.3655666432	22.75652354	0	27.23471492
0.2741749824	1.18809159	0.3655666432	4.478191379	0.456958304	6.94576622	0.0913916608	9.778907705	0.1827833216	12.88622417	0.0913916608	16.35910728	0.3655666432	23.67044015	0	27.5088899
0.456958304	1.462266573	0.3655666432	4.660974701	0.456958304	7.128549542	0.0913916608	10.14447435	0	13.25179082	0.0913916608	16.90745725	0.3655666432	24.12739845	0	27.60028156
0.456958304	1.827833216	0.3655666432	5.117933005	0.5483499648	7.311332864	0.0913916608	10.32725767	0	13.5259658	0.1827833216	17.36441555	0.3655666432	24.49296509	0	27.78306488
0.1827833216	2.376183181	0.3655666432	5.75767463	0.5483499648	7.676899507	0.0913916608	10.60143265	0	13.61735746	0.1827833216	17.82137386	0.3655666432	25.22409838	0	27.87445654
0.0913916608	2.558966502	0.3655666432	5.75767463	0.2741749824	8.225249472	0.0913916608	10.69282431	0	14.07431576	0.1827833216	18.73529046	0.2741749824	25.68105668		
0.0913916608	2.741749824	0.3655666432	5.940457952	0.1827833216	8.499424454	0.0913916608	11.24117428	0	14.43988241	0.1827833216	19.74059873	0.1827833216	26.32079831		

maxX	0.5483499648
maxY	27.87445654
xorigin	yorigin
29.82	29.67
Axial Strain	-0.018057
Lateral Strain	28.67
Poisson's Ratio (v)	0.000630

Figure 10b: Excel Analysis of Displacement Change of Data Prusa Lattice 8 'Spring' & Calculations of Axial Strain, Lateral Strain & Poisson's Ratio

3) Figure 10c: Hourglass Lattice

The positive Poisson's ratio in ***Figure 10c*** reflects conventional material behavior. Axial and lateral strain measurements demonstrate moderate energy absorption, with the lattice contracting laterally under compression. This characteristic makes it suitable for applications requiring a balance between load bearing and stress dissipation.

Overall, Poisson's ratio calculations provide critical insights into the mechanical behavior of each lattice type, validating their suitability for specific orthotic applications.

I. Discussion

A. *Comparative Analysis between Lattice Patterns*

The study's findings indicate that lattice geometry significantly affects mechanical performance. Hexagonal lattices provide superior uniformity in stress distribution, spring lattices excel in energy absorption, and hourglass lattices offer targeted support through auxetic behavior. These distinctions underscore the importance of tailoring lattice designs to specific orthotic requirements.

B. *Stress-Strain Analysis*

The stress-strain curves reveal critical insights into lattice deformation under load. Gradient density configurations demonstrate enhanced strain uniformity, reducing the risk of localized stress failures. The comparison between slicing presets further emphasizes the role of manufacturing precision in achieving desired mechanical properties.

C. *Poisson Ratio Ramifications*

Tuning Poisson's ratios enables customized deformation behaviors, with positive ratios offering cushioning, zero ratios providing stability, and negative ratios enhancing support. This adaptability is crucial for addressing the diverse biomechanical needs of diabetic patients.

D. *Lattice Performativity*

The study validates the effectiveness of gradient density and apex angle modifications in optimizing lattice performance. These innovations improve insole durability and patient comfort, advancing the field of diabetic ulcer orthotics.

E. *Printer Influence on Mechanical Properties*

The comparison between Bambu and Prusa slicers highlights the trade-offs between speed and precision. While Bambu offers rapid prototyping, Prusa's higher resolution ensures research-grade accuracy, making it the preferred choice for detailed lattice analysis.

II. Conclusion

This study demonstrates the potential of lattice structures in optimizing orthotic insoles for diabetic ulcer management. By leveraging advanced design and fabrication techniques, it is possible to enhance mechanical properties, ensuring effective pressure redistribution and support. Future research should explore material durability and long-term performance to further refine these innovations.

III. Reference List

3D DISTRIBUTED (n.d.). *CoreXY Kinematics - 3D Distributed*. [online] 3ddistributed.com. Available at: https://3ddistributed.com/corexy-3d-printer/corexy-kinematics/.

Aryabhat Darnal, Shahid, Z., Deshpande, H., Kim, J. and Muliana, A. (2023). Tuning mechanical properties of 3D printed composites with PLA:TPU programmable filaments. *Composite structures*, 318, pp.117075–117075. doi:https://doi.org/10.1016/j.compstruct.2023.117075.

Babamiri, B.B., Barnes, B., Soltani-Tehrani, A., Shamsaei, N. and Hazeli, K. (2021). Designing additively manufactured lattice structures based on deformation mechanisms. *Additive Manufacturing*, 46, p.102143. doi:https://doi.org/10.1016/j.addma.2021.102143.

Barefoot Filament (2024). *barefilament - Google Search*. [online] Google.com. Available at: https://www.google.com/search?q=barefilament&oq=barefilament&gs_lcrp=EgZjaHJvbWUyBggAEEUYOTIHCAEQLhiABDINCAIQLhivARjHARiABDIHCAMQABiABDIHCAQQABiABDIGCAUQRRg9MgYIBhBFGD0yBggHEEUYPNIBCDM5OThqMGo0qAIAsAIA&sourceid=chrome&ie=UTF-8 [Accessed 12 Jan. 2025].

BYJU'S (n.d.). *Poisson's Ratio - Longitudinal Strain and Lateral Strain | BYJU'S*. [online] BYJUS. Available at: https://byjus.com/physics/poissons-ratio/.

Danko, M., Sekac, J., Dzivakova, E., Zivcak, J. and Hudak, R. (2023). 3D Printing of Individual Running Insoles – A Case Study. *Orthopedic Research and Reviews*, [online] Volume 15, pp.105–118. doi:https://doi.org/10.2147/orr.s399624.

Dey, A.K. (n.d.). *Poisson's Ratio-Formula, Significance, Equation, Example*. [online] What is Piping. Available at: https://whatispiping.com/poissons-ratio/.

James Biggar (2024). *Two Trees SK1 High Speed CoreXY 3D Printer*. [online] YouTube. Available at: https://www.youtube.com/watch?v=QKnOJ3JYbDM [Accessed 12 Jan. 2025].

Kanna, A. and Bala Vaidhyanathan (2024). Additive Manufacturing of Smart Footwear Components for Healthcare Applications. *Micromachines*, [online] 16(1), pp.30–30. doi:https://doi.org/10.3390/mi16010030.

Lempriere, B.M. (2024). Poisson's ratio in orthotropic materials. | AIAA Journal. *AIAA Journal*. [online] doi:https://doi.org/10.2514/aiaaj.1968.6.issue-11;journal:journal:aiaaj;website:website:aiaa-site;wgroup:string:AIAA.

Liu, K., Han, L., Hu, W., Ji, L., Zhu, S., Wan, Z., Yang, X., Wei, Y., Dai, Z., Zhao, Z., Li, Z., Wang, P. and Tao, R. (2020). 4D printed zero Poisson's ratio metamaterial with switching function of mechanical and vibration isolation performance. *Materials & Design*, [online] 196, p.109153. doi:https://doi.org/10.1016/j.matdes.2020.109153.

Nitta, K. and Yam, M. (2012). Poisson's Ratio and Mechanical Nonlinearity Under Tensile Deformation in Crystalline Polymers. *InTech eBooks*. [online] doi:https://doi.org/10.5772/34881.

Perry, S., Huayamave, V., Gonzalez, B., Nadeau, Z. and Rodriguez, R. (2022). *Tensile Testing of 3D Printed TPU Samples for Pediatric Biomaterial Applications*. [online] Available at: https://commons.erau.edu/cgi/viewcontent.cgi?article=1008&context=panasomm.

Prusa Research and Prusa, J. (2025). *Mesh bed leveling | Prusa Knowledge Base*. [online] Prusa3d.com. Available at: https://help.prusa3d.com/article/mesh-bed-leveling_112163 [Accessed 12 Jan. 2025].

Qi, H.J. and Boyce, M.C. (2005). Stress–strain behavior of thermoplastic polyurethanes. *Mechanics of Materials*, 37(8), pp.817–839. doi:https://doi.org/10.1016/j.mechmat.2004.08.001.

ruiraptor (2020). *HOW TO Level your 3D Printer's BED Like a PRO / Mesh Bed Leveling*. [online] YouTube. Available at: https://www.youtube.com/watch?v=9AZy8beDQqg [Accessed 12 Jan. 2025].

Sarinnapakorn, V., Sunthorntepwarakul, T., Deerochanawong, C., Niramitmahapanya, S. and Napartivaumnuay, N. (2016). Prevalence of Diabetic Foot Ulcers and Risk Classifications in Type 2 Diabetes Mellitus Patients at Rajavithi Hospital. *J Med Assoc Thai*, 99, p.99.

Sterman, Y., Solav, D., Rosen, N., Saffuri, E. and Shmilov Zaritsky, L. (2024). Custom orthotic insoles with gradual variable stiffness using 3D printed spacer technique. *Virtual and Physical Prototyping*, 19(1). doi:https://doi.org/10.1080/17452759.2024.2336151.

Zoboli, L., Bianchi, D., Falcinelli, C. and Gizzi, A. (2024). Improving the manufacturing of 3D printed insoles through a combined experimental and topology optimization approach. *Mechanics of Advanced Materials and Structures*, 31(30), pp.12636–12650. doi:https://doi.org/10.1080/15376494.2024.2326667.